

UV-Induced Photopatterning of the Thermoresponsive Properties of a Poly(ethylene glycol)methylether acrylate-co-poly(*N*-isopropylacrylamide) Hydrogel

Qian-Pu Cheng, Nikolaj K. Mandsberg, Pavel A. Levkin,* and Shan-hui Hsu*

Photopatterning offers a versatile and precise approach for modifying surface properties, making it a valuable technique in material design. Recent research demonstrates that polymer swelling can significantly enhance photodegradation, facilitating topographical patterning. Herein, this concept in stimuli-responsive hydrogels is explored, focusing on the thermoresponsive poly(ethylene glycol) methylether acrylate-co-poly(*N*-isopropylacrylamide) (PPEGA–PNIPAM) hydrogel. Surprisingly, it is observed that UV exposure not only partially degrades the hydrogel but also diminishes its thermal responsiveness. This effect enables selective deactivation of responsive properties of the PPEGA–PNIPAM, allowing for spatially defined variations in thermomechanical behavior through photolithography. By using these spatial differences, the hydrogel is programmatically transformed into a thermoresponsive actuator via a single-step photopatterning process, demonstrating a potential application of UV-induced change of thermoresponsiveness. Furthermore, incorporating gelatin methacrylate enhances biocompatibility, suggesting new possibilities for developing thermoresponsive bioactuators. Thus, the results demonstrate the potential of UV-induced modulation of stimuli-responsive properties of hydrogels and present new opportunities for creating multifunctional materials with tailored properties.

lies in their responsiveness to stimuli such as temperature, pH, and light.^[3] The responsiveness of hydrogel is attributed to the ability to absorb and release water, leading to pronounced swelling and contraction. Furthermore, the design and mechanism of hydrogel actuators play a pivotal role in determining their efficacy.^[4] Through precise engineering, hydrogels can be tailored to selectively respond to specific stimuli.^[5] This adaptability makes hydrogel actuators highly promising for diverse applications, including biomedical devices^[6] and drug delivery systems^[7] to soft robotics and adaptive structures.^[8] As the development of hydrogel actuators progresses, their unique combination of responsiveness and versatility paves the way for innovative technological advancements across multiple fields.

Temperature-responsive and light-responsive hydrogels have emerged as advanced platforms capable of intelligently reacting to environmental stimuli.^[9] These hydrogels possess the ability to undergo


significant physical changes when exposed to specific temperatures or light wavelengths. Temperature-responsive hydrogels exhibit the unique property of undergoing a reversible phase transition in response to variations in temperature, which allows the hydrogel to act as responsive matrices in applications such as drug delivery,^[10] tissue engineering,^[11] and controlled release systems.^[12] Common polymers employed in fabricating thermoresponsive hydrogels include poly(*N*-isopropylacrylamide) (PNIPAM). PNIPAM undergoes a coil-to-globule transition near

1. Introduction

Hydrogels with exceptional responsiveness to environmental stimuli have emerged as a captivating class of materials in the field of actuators. Actuators are devices designed to convert various forms of energy into mechanical motion.^[1] Hydrogels, with their unique ability to undergo significant volume changes in response to external factors, are gaining prominence in this field.^[2] One of the distinctive features of hydrogels as actuators

Q.-P. Cheng, S. Hsu
Institute of Polymer Science and Engineering
National Taiwan University
No. 1, Sec. 4 Roosevelt Road, Taipei 10617, Taiwan, R.O.C.
E-mail: shhsu@ntu.edu.tw

N. K. Mandsberg, P. A. Levkin
Institute of Biological and Chemical Systems-Functional Molecular systems (IBCS-FMS)
Karlsruhe Institute of Technology
Kaiserstraße 12, 76131 Karlsruhe, Germany
E-mail: levkin@kit.edu

 The ORCID identification number(s) for the author(s) of this article can be found under <https://doi.org/10.1002/sstr.202400560>.

P. A. Levkin
Institute of Organic Chemistry
Karlsruhe Institute of Technology
76131 Karlsruhe, Germany

© 2025 The Author(s). Small Structures published by Wiley-VCH GmbH. This is an open access article under the terms of the Creative Commons Attribution License, which permits use, distribution and reproduction in any medium, provided the original work is properly cited.

S. Hsu
Institute of Cellular and System Medicine
National Health Research Institutes
Miaoli 350401, Taiwan, R.O.C.

DOI: 10.1002/sstr.202400560

physiological temperatures, making it particularly suitable for biomedical applications.^[13] On the other hand, light-responsive hydrogels leverage the unique properties of photoresponsive polymers to trigger changes in their structure or properties upon exposure to specific wavelengths of light.^[14,15] Photoresponsive polymers, such as azobenzene-containing polymers^[16] and acrylate group-based polymers,^[17] are frequently used for light-responsive hydrogel systems as they can undergo reversible photoisomerization or irreversible polymerization upon exposure to UV or visible light. In particular, poly(ethylene glycol) methacrylate (PEGMA)-based hydrogel exhibits photodegradability as revealed in previous literature, which stems from the susceptibility of the hydrated PEG and poly(meth)acrylate chains to cleavage upon exposure to high intensity UVC light.^[18] This photodegradability enables precise control over the degradation of hydrogels, offering a pathway to environmentally responsive and programmable material behaviors. The PEGMA displays favorable attributes of PEG, such as biocompatibility and hydrophilicity.^[19] Generally, the exact choice of polymer depends on the specific requirements of the application, considering factors such as biocompatibility, tunable responsiveness, and stability.

Designing hydrogel actuators requires a multidisciplinary approach, combining materials engineering and responsive systems to harness the inherent properties of hydrogels for controlled and dynamic mechanical responses. Hydrogel actuator design centers on forming a three-dimensional network using materials such as PNIPAM, polyacrylic acid, or PEG-based hydrogels, selected for their ability to undergo significant volume changes in response to external stimuli.^[20] Meanwhile, the spatial arrangement and geometric design of hydrogel actuators play a pivotal role in determining their mechanical responses.^[21] Engineered structures, such as bilayers or gradient patterns within the hydrogel, contribute to controlled directional actuation.^[22] Hydrogels with a carefully designed structure can achieve complex and programmable movements. Innovations in hydrogel actuators focus on improving responsiveness, durability, and biocompatibility, paving the way for applications in biomedical fields such as wearable devices, artificial muscles, and in vitro simulation platforms.^[23–25]

Here, we successfully develop a PPEGA–PNIPAM (PN) hydrogel actuator utilizing a photodegradable poly(ethylene glycol) methyl ether acrylate (PEGA) hydrogel system combined with temperature-responsive PNIPAM. The PPEGA–PNIPAM hydrogel exhibits thermal responsiveness and can be partially degraded by UVC irradiation. Most notably, photodegradation also suppresses the hydrogel's thermal responsiveness, enabling programmable actuation capabilities within a single-layer hydrogel. By employing different grating patterns, photodegraded (i.e., passive) regions were introduced, resulting in hydrogel structures with tunable contraction or bending. This study systematically investigates the photodegradation behavior, thermal responsiveness, actuation performance, and biocompatibility of the PPEGA–PNIPAM hydrogel. Biocompatibility tests using C2C12 muscle cells assess the potential of PPEGA–PNIPAM hydrogels as platforms for in vitro muscle tissue simulation, opening new possibilities for biomedical applications.

2. Results and Discussion

2.1. Photodegradation and Temperature Responsiveness of PN Hydrogel Thin Films

The design of the PN hydrogel drew inspiration from previous research on photodegradable hydrogels^[26] and PNIPAM-based hydrogels.^[27] The combined system aimed to exhibit a dual-responsive behavior, involving both photoresponsiveness and thermoresponsiveness. The PN hydrogel was initially prepared as a uniformly responsive material and then transformed into a programmable responsive hydrogel through selective photodegradation and photopatterning (**Figure 1A**). The compositions of various PN hydrogels and the PEGA hydrogel control group are shown in **Table 1**. The compositions were adjusted and optimized for this study based on previous research.^[18] The possible network structure of the PN hydrogel is depicted in **Figure 1B**. Photocrosslinking between PEGA and NIPAM occurs upon exposure to UVA light (365 nm), while the PEGA–PNIPAM network is observed to degrade under UVC light (254 nm). The continuous network between PEGA and NIPAM is assumed to resemble a copolymer. After photodegradation, the PN network is expected to cleave, resulting in fragments of PPEGA–PNIPAM. This fragmentation is supported by the IR spectra of photocrosslinked and photodegraded PN hydrogels, which show no significant differences in characteristic peaks (**Figure S1**, Supporting Information).

The preparation process of photodegradable PN hydrogels is illustrated in **Figure 2A**. The preparation of PN hydrogel thin films involved the use of channels formed by slides and aligned tapes. The polymerization of PEGA and NIPAM monomer was performed under UVA exposure for 2 min. The resulting photocrosslinked PN hydrogel was then immersed in DI water overnight to allow for swelling, which expanded the polymer chains and network. Subsequently, the swollen hydrogel underwent photodegradation under UVC exposure at a constant temperature of 20 °C for 1 h. Maintaining a constant temperature of 20 °C for the PN hydrogel ensures that no phase transition occurs under UV exposure heat, which is important as PNIPAM has a lower critical solution temperature of 32 °C. The height of the swollen and photodegraded PN hydrogels was measured using a camera to assess the degree of photodegradation. The swelling ability and thickness of PN hydrogel can influence photodegradation efficiency, as previously reported.^[18] PN hydrogels with different compositions exhibit high swelling ratios and gel fractions, indicating a stable crosslinking network, as detailed in **Table 1**. In **Figure S2A**, Supporting Information, the swollen PN hydrogel thin film measured a height of 0.965 mm, while the thin film postphotodegradation (UVC exposure for 1 h) measured a height of 0.670 mm. The degree of photodegradation against UVC exposure time, illustrated in **Figure S2B**, Supporting Information, depicts the remaining percentage of PN hydrogel thin films across the three groups. A higher NIPAM ratio in the PN hydrogel was found to inhibit photodegradability. NIPAM monomers are presumed to act as crosslinkers or short bridges between PEGA polymers in the PN system. A higher NIPAM ratio in the PN hydrogel leads to stronger and longer crosslinkages between PEGA polymers compared to a lower NIPAM ratio. The PN hydrogel group containing 2 wt%

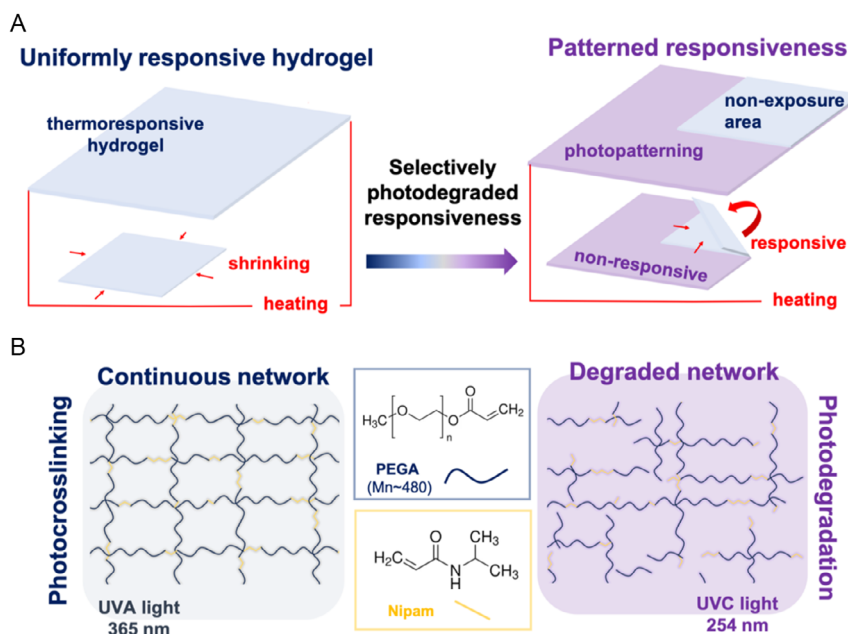


Figure 1. Schematic illustrating the concept and mechanism of selective photodegradation for programmable material responsiveness. A) PEGA–PNIPAM (PN) hydrogel was prepared as a uniformly responsive hydrogel and selectively photodegraded to create programmable responsiveness. B) Chemical structures between PEGA and NIPAM illustrate anticipated crosslinks following UVA exposure (365 nm) and cleaved polymer chains after UVC exposure (254 nm).

Table 1. Swelling ratios and gel fractions of PEGA and PN hydrogels. The swelling ratio was calculated using the formula $(W_s/W_p) \times 100\%$, where W_p is the initial hydrogel weight and W_s is the weight after swelling. For the gel fraction, samples were lyophilized, weighed (W_i), immersed in deionized (DI) water at 25 °C for 24 h, and then freeze-dried and weighed again (W_f). The gel fraction was determined using the equation $(W_f/W_i) \times 100\%$.

Sample	PEGA [32 wt%]	PEGA:NIPAM [31 wt%:1 wt%]	PEGA:NIPAM [30 wt%:2 wt%]	PEGA:NIPAM [28 wt%:4 wt%]
Swelling ratio [%]	523 ± 37	586 ± 24	551 ± 16	542 ± 28
Gel fraction [wt%]	73 ± 2	77 ± 2	71 ± 2	72 ± 2

of NIPAM exhibited $\approx 40\%$ thickness reduction through photodegradation, similar to the group with 1 wt% of NIPAM. The 2 wt% group was selected for further experiments.

The PN hydrogel thin films exhibit partial photodegradability and derivative properties, as evidenced by gross obversion, Small angle X-ray scattering (SAXS) analyses, and rheology. The photodegradation of the PN hydrogel thin film significantly affects its thermoresponsive ability. A comparison of the thermoresponsiveness of the PN hydrogel at 40 °C across the groups after photocrosslinking, after swelling, and after photodegradation revealed noticeable shrinking in the group after swelling, but only minor change in the group after photodegradation, as shown in Figure 2B. The thermoresponsive ability of the PN hydrogels was quantified using the deswelling ratio (Table 2). The PN hydrogels exhibited over 30% deswelling ratio under 40 °C heating and above 95% reswelling ratio at 25 °C. The deswelling ratio of the PN hydrogel thin film after photodegradation approached 2%, indicating the near-complete loss of thermoresponsiveness.

The microstructure of the PN hydrogel thin film after photocrosslinking and photodegradation at 25, 40, and 70 °C was inferred from SAXS profiles. A comparison of the SAXS profile for the photodegraded PN hydrogel with that of the photocrosslinked PN hydrogel showed a decrease in intensity starting from

the q -value of 0.009 (Figure 2C(i)). This q -value corresponds to an estimated scale of 69.7 nm. The observed decrease in intensity suggests that photodegradation of the PN hydrogel occurs due to network cleavage at length scales shorter than ≈ 69.7 nm (Figure 2C(ii)). The thermoresponsiveness of the photocrosslinked PN hydrogel is evident from the increase in intensity in the q -range from 0.007 \AA^{-1} (corresponding to 89.7 nm) to 0.07 \AA^{-1} (8.97 nm) observed in the SAXS profiles as the temperature increases from 25 °C to 40 °C (Figure 2D(i)). It is also noted that no further changes to the profiles are observed when the temperature is increased further from 40 to 70 °C. Together, this suggests that the network of the photocrosslinked PN hydrogel tightens within the range of 89.7–8.97 nm during heating (Figure 2D(ii)). In contrast, the SAXS profiles for the photodegraded PN hydrogel show no difference upon heating (Figure 2E(i)). This indicates that the photodegraded PN hydrogel does not exhibit any thermoresponsive behavior in terms of network structure (Figure 2E(ii)). The results from the SAXS analysis support the relationship between thermoresponsiveness and photodegradation of the PN hydrogel thin film. These fundamental mechanism studies for microstructure–property–functionality of the PN hydrogel thin film corroborate its potential as a programmable actuator.

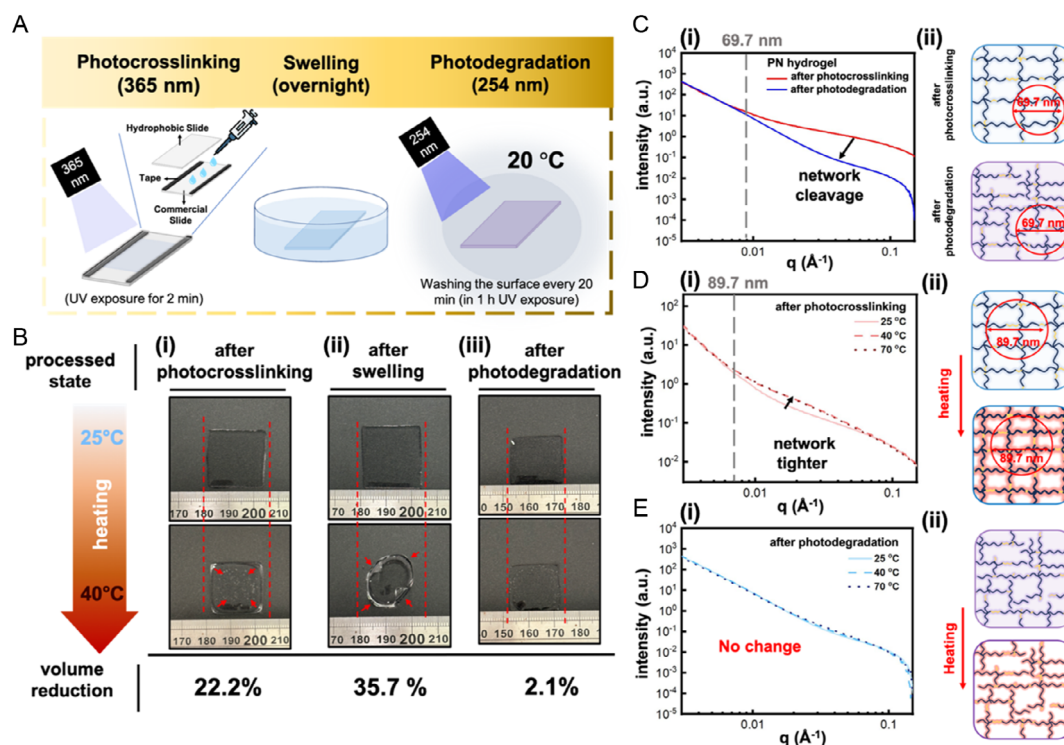


Figure 2. Preparation, thermoresponsive ability, SAXS analysis, and structural hypothesis of PN hydrogel thin film. A) Hydrogel thin films were prepared using photocrosslinking (UVA, 365 nm, 2 min), swelling overnight, and photodegradation (UVC, 254 nm, 20 °C, 1 h). B) Observations: i) slight shrinkage in the photocrosslinked hydrogel, ii) swollen hydrogel rolled into a tube, and iii) no change in the photodegraded hydrogel. C) SAXS analysis: i) decreased intensity postphotodegradation from $q = 0.009$ (69.7 nm) and ii) structural collapse suggested in postphotodegradation network. D) Heating effects postphotocrosslinking: i) increased intensity from $q = 0.007$ (89.7 nm) to 0.07 (8.97 nm) and ii) network tightening during heating. E) Heating effects postphotodegradation: i) no change in SAXS profiles and ii) no thermoresponsive behavior observed.

Table 2. The deswelling ratio and reswelling ratio of PN hydrogels. Temperature-responsive behavior of PN hydrogels, evaluated by deswelling and reswelling ratios. The deswelling ratio at 40 °C was calculated as $[(W_s - W_d)/W_s] \times 100\%$, where W_s and W_d are the hydrogel weights after swelling and deswelling, respectively. The reswelling ratio was determined by immersing the deswelled hydrogel in 25 °C DI water and calculated as $(W_r/W_s) \times 100\%$, where W_r is the weight after reswelling.

Experimental group	PEGA:NIPAM [31 wt%:1 wt%]	PEGA:NIPAM [30 wt%:2 wt%]	PEGA:NIPAM [28 wt%:4 wt%]
Deswelling ratio [%]	31 ± 1	36 ± 1	40 ± 1
Reswelling ratio [%]	98 ± 0.4	99 ± 0.1	95 ± 0.2

The storage modulus of the PN hydrogel after photocrosslinking was measured at 353 Pa (Figure 3A), with a decrease in modulus observed following both swelling (265 Pa, Figure 3B) and photodegradation (98 Pa, Figure 3C). During strain sweep analysis, damage to the photocrosslinked PN hydrogel was observed at 900% strain (Figure 3D), while the swollen and photodegraded PN hydrogels experienced damage at the strain of 490% (Figure 3E) and 190% (Figure 3F), respectively. Rheological analysis of the PN hydrogel indicates that the crosslinking and structure weakening after swelling and photodegradation. The results

of rheology for the PN hydrogels reveal the mechanical properties after photocrosslinking and photodegradation.

The photodegradation mechanism of the hydrogel under 254-nm UV light is primarily attributed to Norrish type I cleavage of ester bonds within the polymer network. This cleavage leads to decrosslinking of the polymer network and alters its thermoresponsive properties. Photodegradation was previously investigated,^[28,29] where the effects of UV irradiation on swollen hydrogels and microgels were studied using techniques such as UV-vis spectroscopy, nuclear magnetic resonance (NMR), and gel permeation chromatography (GPC). The reduced susceptibility of PNIPAM-based hydrogels to UV-induced degradation, along with the lower reduction in deswelling ratio compared to PEG-based systems, suggests that the cleavage of PEG chains (ester bonds) is more efficient than that of amide groups. Overall, disruption of the three-dimensional network of the hydrogel alters its thermoresponsive properties, deswelling behavior, and mechanical integrity (Figure 2B and 3B,C).

It should be mentioned that prolonged exposure to UV irradiation that induces bond cleavage, degradation, and reduction of thermoresponsive properties of the hydrogel may also affect the mechanical properties of the remaining hydrogel. The latter may deteriorate the lifespan and reduce usage cycles of the produced hydrogel material.^[30]

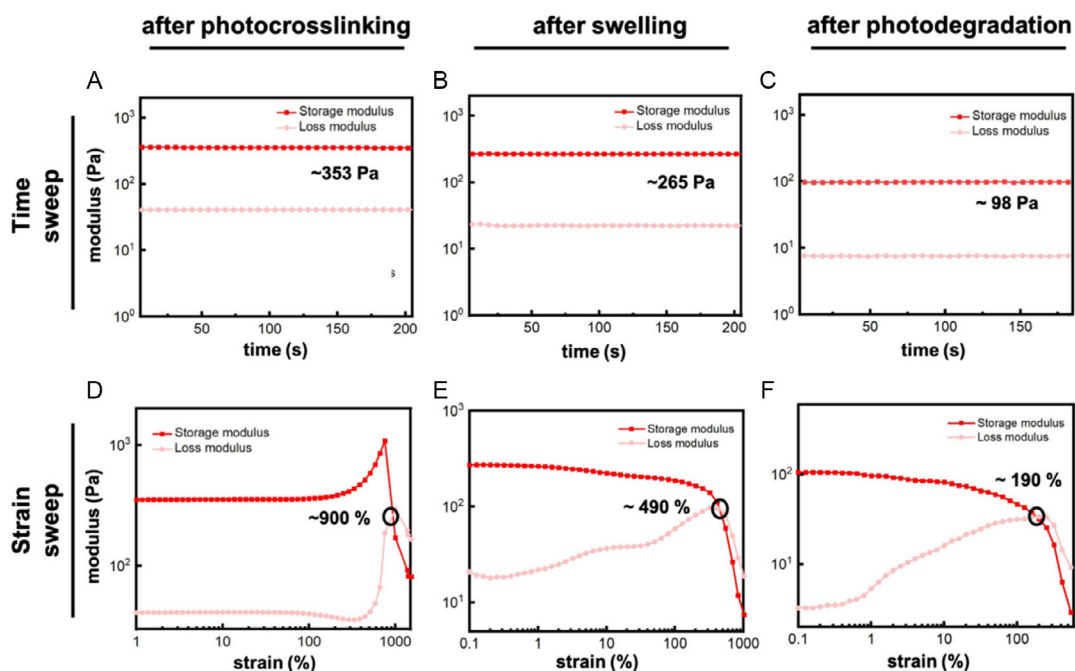


Figure 3. Rheological analysis of PN hydrogel (30 wt% of PEGA:2 wt% of NIPAM). A) Time sweep of hydrogel during photocrosslinking conducted under 1% strain and 1 Hz frequency using an in situ UV system. B,C) Time-dependent storage and loss moduli (G' and G'') of hydrogels after swelling and photodegradation were measured under 1% strain and 1 Hz frequency. D–F) Strain-dependent storage and loss moduli (G' and G'') of hydrogels postphotocrosslinking, swelling, and photodegradation processes were examined under dynamic strain at a frequency of 1 Hz.

2.2. UV Pattern Design and Actuation Behavior on a Single Layer of the PN Hydrogel Thin Film

Recent progress in manufacturing hydrogel actuators with anisotropic structures has included bilayer structures, gradient structures, patterned structures, and oriented structures.^[4] The materials in these methods were mostly prepared by combining two hydrogel systems and inorganic additives.^[31–35] Here, in contrast, we fabricated the PN hydrogel actuator from a monolayer hydrogel system, as shown in Figure S3, Supporting Information. The PN hydrogel thin film was covered with a customized photomask, and the uncovered area was exposed to UVC light for an hour to create a passive area (i.e., photodegraded area), as illustrated in Figure 4A. The PN hydrogel thin films with simple patterns were used to demonstrate the actuation principle. Two examples are shown, where either 1) half of a rectangular hydrogel thin film or 2) a quarter of a square hydrogel thin film was left active, both cases showing noticeable selective bending and shrinking upon heating (Figure 4B,C). The actuating performance of the patterned hydrogel thin films indicated controllable actuation by inhibiting the thermoresponsive ability (Figure S4, Supporting Information).

Moreover, the deswelling ratios of the PN hydrogel thin film under different exposure times for photodegradation (1, 5, 10, 30, and 60 min) demonstrated a gradual inhibition of thermoresponsive ability (Figure 4D). Depicting the deswelling ratio against different exposure times provides guidance for controllably adjusting the thermoresponsiveness of the PN hydrogel thin film. A programmable actuation of the PN hydrogel thin film

was achieved using a gradient thermoresponsive ability to perform a sequential reaction in heating and exhibited the reswelling performance after cooling (Figure 4E). Different durations (0, 10, 15, and 20 min) of UVC exposure on the leaf blades of the clover-shaped hydrogel thin film resulted in an ordered, sequential motion during heating (Figure 4F). The actuated hydrogel thin film was subsequently immersed in cool water and reswelled gradually (Figure 4G). The force from the water for reswelling the hydrogel thin film was insufficient to fully unfold the leaves, so they were expanded manually using tweezers, and the excess water was removed using a pipette. The complete heating/cooling cycle of the clover-shaped hydrogel thin film was recorded and is shown in Movie S1, Supporting Information. Moreover, another programmable actuation of the PN hydrogel thin film was performed in a finger shape, which showed sequential withdrawal of the fingers (Figure S5, Supporting Information).

2.3. Growth of C2C12 Myoblast Cells in PN-Based Hydrogel Thin Films

Drawing inspiration from the adaptability and responsiveness of biological systems, hydrogel actuators demonstrate unique capabilities that position them at the forefront of innovation in biomimicry.^[36] The biomimetic design of hydrogel actuators aims to replicate the remarkable features of living organisms. One of the key behaviors that researchers focus on is the hierarchical organization observed in muscle tissue.^[37] While mimicking the intricate structure and function of muscle tissue in vitro is

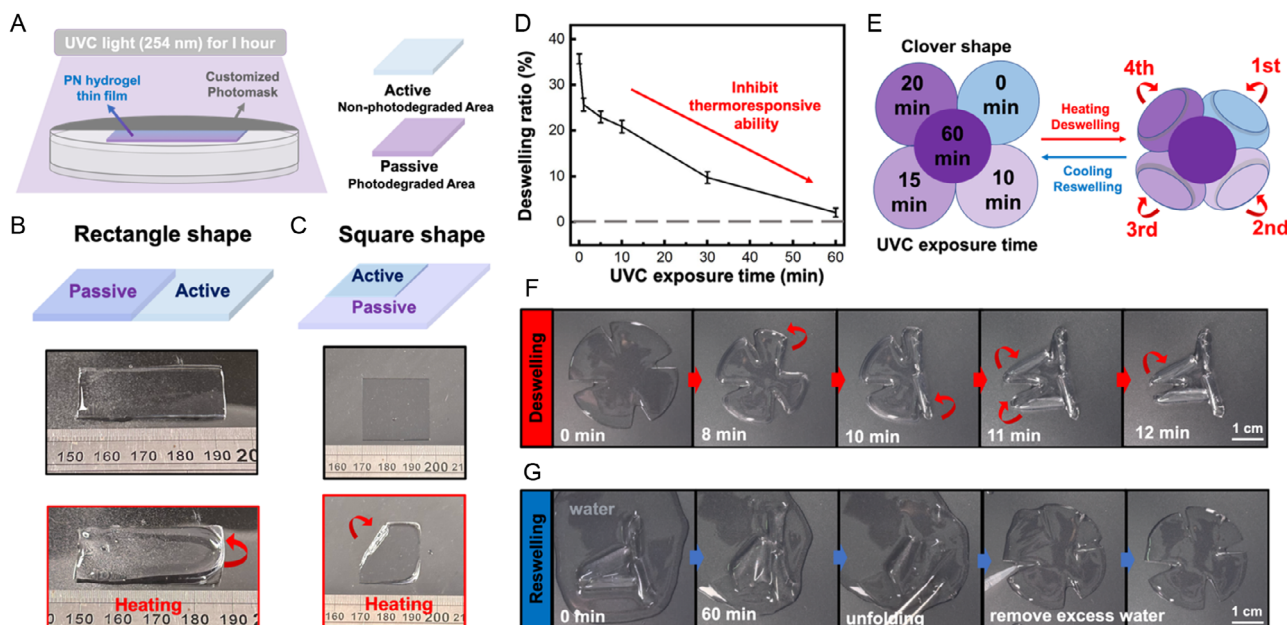


Figure 4. Anisotropic and programmable actuation of PN hydrogel thin film. A) Photodegradation was used to inhibit thermoresponsive behavior, creating passive areas (blue: active, purple: passive). B) Photodegradation on half of a rectangular film caused bending during heating on one side. C) Shrinking occurred at the corners of a square film where photodegradation was not applied. D) Deswelling ratios reflect the impact of UVC exposure on thermoresponsiveness. E) Gradual thermoresponsiveness was induced by varying UVC exposure times, enabling sequential leaf actuation in a clover-shaped film. F) The leaf blades reacted in the programmed order during heating. The actuating speeds of the third and fourth leaves are very similar. G) The hydrogel thin film was immersed in cool water for reswelling. Tweezers and a pipette were used to unfold the leaves and remove the excess water after the hydrogel thin film reswelled.

a formidable challenge, hydrogel actuators offer a versatile solution.^[27,38] The *in vitro* simulation platform of muscle tissue allows researchers to assess the effects of drugs on muscle cells, study the progression of muscle-related diseases, and explore potential therapeutic interventions.^[39,40] The challenges in the field of hydrogel actuators revolve around achieving precise control, customization for specific applications, and biomimetic replication of complex biological structures. The intricacies of muscle movement have received considerable attention, leading to efforts to mimic muscle performance using hydrogel actuators as artificial muscles.^[41–44] Most studies on manufacturing hydrogel actuators have focused on mechanical properties, stimuli-responsive speed, and durability to ensure they are suitable for use as artificial muscles.^[45–47] Therefore, the materials used in these studies generally lack biocompatibility, making it difficult to develop an *in vitro* platform for researching muscle cells or muscle-related diseases within an artificial muscle environment. The gelation of the PN-based hydrogels is primarily achieved through the copolymerization of PEGA and NIPAM, where the polymer chains form a three-dimensional network without the need for an extra covalent crosslinking agent. This approach simplifies the synthesis and reduces potential cytotoxicity associated with some crosslinking agents. Additionally, previous studies on PEGA-based photodegradable hydrogel and gelatin-methacryloyl (GelMA)-based hydrogel actuators have demonstrated the potential for biocompatibility in cell culture.^[19,29] In this study, 2 wt% of GelMA was added to the PN hydrogel system to enhance its biocompatibility (Figure S6,

Supporting Information). The PN-GelMA hydrogel exhibited a high swelling ratio, photodegradation, and thermoresponsive ability as well (Table S2 and Figure S7, Supporting Information). A comparison of the C2C12-embedded PN hydrogel and PN-GelMA hydrogel demonstrated good cell viability of C2C12 cells in the PN-GelMA hydrogel after photocrosslinking, as shown in the live/dead staining in Figure 5A. The PKH67-stained C2C12 cells incubated in the PN hydrogel and PN-GelMA hydrogel, tracked with green fluorescence, revealed expansion of the cells after swelling (Figure 5B). The long-term cell viability of C2C12 cells in the PN-GelMA hydrogel exhibited 150% cell proliferation after 7 days in Figure 5C. A 4 wt% GelMA hydrogel was used as a positive control in cell proliferation experiments. The survival of C2C12 myoblast cells in the PN-GelMA hydrogel presented the potential application as an *in vitro* actuating environment for researching drug effects on muscle cells or muscle-related diseases.

2.4. Overview and Comparison of Our UV-Induced Photodegraded PN Hydrogel with Existing Stimuli-Responsive Hydrogels and Actuators

The typical gradient hydrogel actuator created by photolithography involves a photo-induced crosslinking reaction, which provides tunable mechanical properties and achieves distinct actuation capabilities, such as bending angles or anisotropic actuation behaviors.^[35] Compared to photo-induced surface crosslinking, UV-induced degradation achieves comparable spatial

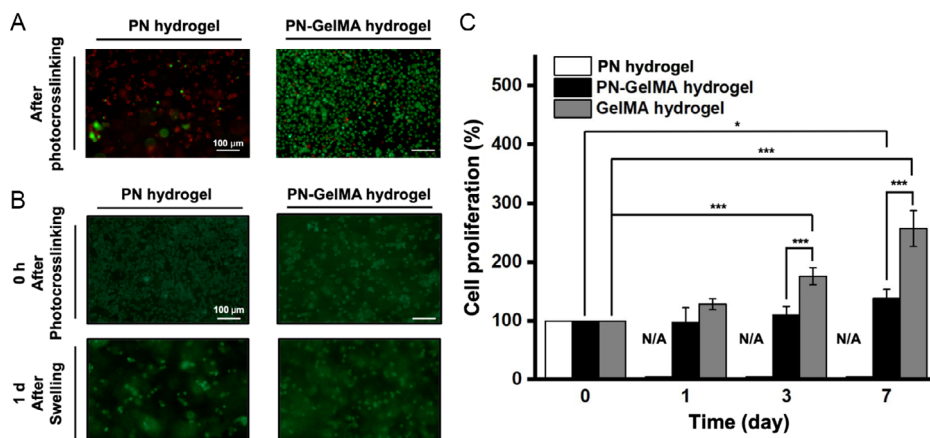


Figure 5. Survival, tracking, and proliferation of C2C12 cells in the PN hydrogel and PN-GelMA hydrogel. A) Cell viability in the hydrogels after photocrosslinking was shown by the live/dead staining of C2C12 cells. B) The PKH67-stained C2C12 cells incubated in the hydrogels for 0 h (after photocrosslinking) and 24 h (after swelling) were captured with green fluorescence for tracking. C) The long-term proliferation of C2C12 cells in PN hydrogel, PN-GelMA hydrogel, and GelMA hydrogel (positive control) was determined by the Cell Counting Kit-8 (CCK-8) assay. * $p < 0.05$ and *** $p < 0.001$ among the indicated groups.

control. In photo-induced surface crosslinking strategies, using two or more materials or precise control of crosslinking degree is typically required to achieve anisotropic actuation. Hydrogels with lower crosslinking densities often face mechanical weaknesses due to the rapid free radical reaction of photocrosslinking. Therefore, using different materials in photo-induced surface crosslinking strategies allows for more stable or predictable mechanical strength, making it a widely adopted approach for achieving spatially specific actuation. While this multimaterial strategy provides stability and predictability, it complicates the fabrication process. In contrast, our PN hydrogel thin-film system achieves comparable spatial control through UV-induced degradation without requiring additional materials or intricate crosslinking control.

While our PN hydrogel thin-film system is, to our best knowledge, the first to demonstrate the integration of photodegradability with inhibition of thermoresponsiveness, there are many other thermoresponsive polymers and hydrogels (Table S3, Supporting Information) of which thermoresponsiveness might be tuned by UV-induced degradation of the polymer network. Nevertheless, not all polymers might be degraded by UV light to the same extent as the swollen PEG-containing hydrogels investigated here, warranting further investigation to explore the broader applicability of this approach to tuning the stimuli-responsive properties.

In order to assess if the observed UV-induced degradation may influence responsive hydrogel systems with other compositions, we synthesized two additional hydrogel variants: PNIPAM-PEGA (15 wt% NIPAM and 5 wt% PEGA) and PEGDA-PNIPAM (30 wt% PEGDA and 2 wt% NIPAM). The PNIPAM-PEGA hydrogel contains a significantly larger fraction of NIPAM (15 wt% vs 1–4 wt% in the previous system), while the PEGDA-PNIPAM is based on the bifunctional PEG making it a more crosslinked PEGDA-based hydrogel, as opposed to the PEGA-NIPAM system investigated above. Both hydrogels were studied for their UV-induced photodegradable properties

assessed by measuring decreases in hydrogel thicknesses (Figure S8, Supporting Information) as well as for their deswelling ratios upon heating to 40 °C before and after photodegradation (Table S4, Supporting Information). Both PNIPAM-PEGA and PEGDA-PNIPAM hydrogels showed thermoresponsive properties before photodegradation with deswelling ratios of 93 and 13.5%, respectively. PNIPAM-PEGA and PEGDA-PNIPAM hydrogels showed a reduction in thickness of 0.75 and 0.3 mm, respectively, after irradiation with 254 nm UV light (22 mW cm^{-2}) for 1 h, demonstrating the photodegradability, while the deswelling ratio reduced only from 93 to 90% in the case of NIPAM-PEGA and from 13.5 to 7% in the case of PEGDA-PNIPAM. These results show that the reduction of thermoresponsive properties is not universal and depends on the composition of the hydrogel. The presence of PEG in the material seems to be important for achieving more efficient reduction of thermoresponsiveness (cf., 13.5–7% vs 93–90% change of deswelling ratio), at least for the PEG-NIPAM systems.

3. Conclusion

In this study, we demonstrated a photodegradation-based method to locally modulate the stimuli-responsive properties of PPEGA-PNIPAM hydrogel. We showed that UV exposure of this hydrogel induces partial degradation of the hydrogel while simultaneously diminishing its thermal responsiveness. This dual effect allows for the selective deactivation of responsive properties, enabling the creation of spatially defined variations in thermomechanical behavior through photolithography. By exploiting these spatial differences, we transformed the hydrogel into a thermoresponsive actuator using a single-step photopatterning process. This approach shows an application of UV-induced changes in thermoresponsiveness, offering a straightforward method to program complex actuation behaviors into hydrogel materials. Furthermore, the incorporation of GelMA enhanced the biocompatibility of the hydrogel,

suggesting promising avenues for developing thermoresponsive bioactuators. Thus, our findings demonstrate the potential of UV-induced modulation in altering temperature-responsive properties. This technique can be used for designing materials with customized properties, providing solutions in areas such as soft robotics, tissue engineering, and responsive surfaces.

4. Experimental Section

Chemicals: NIPAM (99%, Thermo Scientific, USA), poly(ethylene glycol) methyl ether acrylate (PEGA, $M_n \approx 480$, Sigma-Aldrich, Germany), 2,2-azobis(2-methyl-N-(2-hydroxyethyl) propionamide) (VA-086, Wako Chemicals GmbH, Germany), gelatin (type A, 300 bloom, Sigma-Aldrich, USA), methyl acrylic anhydride (MAA, Sigma-Aldrich, Germany), high-glucose Dulbecco's modified Eagle's medium (DMEM, Gibco, USA), fetal bovine serum (FBS, Gibco, USA), penicillin-streptomycin (Caisson), and CCK-8 (CCK-8, Sigma-Aldrich, Japan) were purchased. Gelatin-methacryloyl (GelMA) was synthesized from gelatin and MAA in carbonate-bicarbonate buffer according to a protocol previously reported. The degree of substitution of GelMA was evaluated by ^1H NMR spectroscopy (Bruker Avance-500 Spectrometer).

Preparation and UV Photodegradation of PEGA-PNIPAM (PN) Hydrogel Thin Films: The PN hydrogels were prepared from PEGA and NIPAM. PEGA (31, 30, and 28 wt%) and NIPAM (1, 2, and 4 wt%) solutions were mixed with the photoinitiator VA-086 (2 wt% of solid content). The prepolymer was pipetted onto a commercial slide with a customized channel and covered by a hydrophobic slide. The precursor was exposed to UV light (22 mW cm^{-2} , 365 nm) for 2 min to allow for the hydrogel thin film formation. The photocrosslinked hydrogel thin film was subsequently swollen overnight in DI water. The swollen hydrogel thin film was degraded under UV light (254 nm) for 1 h at a constant temperature of 20 °C. The UV lamp used in our experiments is a UV chamber with a customized temperature controller (UV chamber with customized temperature controller, GB-3501, Ganbow Tech., Taiwan). The UV wavelength used was 254 nm (intensity 22 mW cm^{-2}). After the degradation of the PN hydrogel thin film, we observed significant overall thickness changes using a camera to take the image of the cross section. The remaining percentage was determined by measuring changes at multiple points and calculating the average, ensuring the reliability of our measurements.

Characterization of PN Hydrogel Thin Films: The chemical composition of crosslinked hydrogel and photodegraded hydrogel was confirmed using Fourier transform infrared spectroscopy (PerkinElmer, USA) and scanned at a resolution of 8 cm^{-1} from 400 to 4000 cm^{-1} . The gel fraction of various PN hydrogels and the control group PEGA hydrogel with 32 wt% were estimated as the degree of chemical crosslinking. The samples were lyophilized for 24 h and weighed (W_i). Subsequently, the lyophilized samples were immersed in 25 °C DI water for 24 h. The resulting samples were then freeze-dried for another 24 h and weighed (W_f). The gel fraction was calculated by equation $(W_f/W_i) \times 100\%$. The height of the swollen hydrogel thin film and the photodegraded hydrogel thin film were imaged using a contact angle meter (WCA instrument, First Ten Angstroms, USA) and measured with the ImageJ software.

SAXS experiments for the PN hydrogels were conducted at the beamline 23A of the Taiwan Light Source (TLS 23A) in the National Synchrotron Radiation Research Center located in Hsinchu, Taiwan. The photon energy of the equipment was set to 8 keV, and the scattering vector (q values) ranged from 0.004 to 0.4 \AA^{-1} . The profiles of photocrosslinked PN hydrogel and photodegraded PN hydrogel were measured at 25 °C. Temperature-dependent profiles were obtained at 25 °C, 40 °C, and 70 °C, with the sample allowed to equilibrate for 10 min after each temperature change to ensure thermal stability.

Rheological properties of the PN hydrogels during photocrosslinking and postswelling and photodegradation were assessed using a rheometer (HR-2, TA Instruments). All experiments were conducted at 25 °C employing a 20 mm parallel plate geometry, and an in situ UV light platform (HR-2, TA Instruments) was utilized, except for the time and strain sweeps.

During photocrosslinking, the storage modulus (G') and loss modulus (G'') were monitored over time under a UV lamp (22.4 mW cm^{-2}) at a constant frequency of 1 Hz and an oscillatory strain of 1%. Additionally, the storage modulus (G') and loss modulus (G'') of the swollen hydrogel and photodegraded hydrogel were determined at a constant frequency of 1 Hz and an oscillatory strain of 1%. A dynamic strain sweep was performed at a constant frequency of 1 Hz within the strain range of 0.1–1500%.

Swelling and Temperature Responsiveness of PN Hydrogel Thin Films: Swelling ratios of the PN hydrogels in DI water were measured at 25 °C. Initially, the hydrogel was weighed (W_p) and then immersed into water for a specified duration. After swelling, the weight of the hydrogel (W_s) was measured following the removal of excess water around the hydrogel and container. The swelling ratio was obtained from the formula

$$(W_s/W_p) \times 100\% \quad (1)$$

The temperature-responsive ability of PN hydrogels was evaluated based on the deswelling ratio at 40 °C. The swollen hydrogel was initially weighed (W_s) at 25 °C. Subsequently, the hydrogel was heated to an equilibrium temperature of 40 °C, and its weight (W_d) was measured after removing the excess of water. The deswelling ratio was calculated using equation

$$[(W_s - W_d)/W_s] \times 100\% \quad (2)$$

The deswelled PN hydrogel was immersed in 25 °C DI water to assess the reswelling ratio. The weight (W_r) of reswelled hydrogel was measured following the removal of excess water around the hydrogel. The reswelling ratio was calculated using the equation

$$(W_r/W_s) \times 100\% \quad (3)$$

UV Pattern Design and Actuation Experiment: Patterning of the hydrogel thin films was conducted by irradiation of UV light (22 mW cm^{-2}) for 1 h under various shapes of customized photomasks. The active area of the hydrogel thin film was the nonphotodegraded part. The external heater (40 °C) triggered the actuation of the hydrogel thin film to achieve anisotropic shrinking.

The hydrogel thin films were shaped into finger and flower shapes to mimic finger counting and flower blooming gestures. These shaped hydrogel thin films were subjected to varying exposure times (10, 15, 20, and 60 min) of UVC light to induce gradient thermoresponsiveness and observe their actuation behaviors.

Cell Viability of PN-Based Hydrogel Thin Films: The C2C12 mouse myoblast cell line derived from mouse musculus was employed for 3D cell culture. Cells were cultured in high-glucose DMEM supplemented with 10% FBS and 1% penicillin-streptomycin. The cultured cells were maintained at 37 °C and a humidified atmosphere containing 5% CO_2 . The cell culture medium was refreshed every 2–3 days.

Cell proliferation within hydrogels was assessed using the CCK-8 assay. Following trypsinization, cells ($6 \times 10^6 \text{ cells mL}^{-1}$) were combined with PN solution and PN-GelMA solution, respectively. The photoinitiator VA-086 was used at 2 wt% of solid content, and the PEGA, NIPAM, and GelMA were used at 30, 2, and 2 wt%, respectively. These solutions were then dispensed into the wells of a 24-well plate and exposed to UV light (365 nm , 22 mW cm^{-2}) for 2 min. The hydrogel formed a volume of $400 \mu\text{L}$ and a weight of $0.4139 \pm 0.003 \text{ g}$ with a cylinder and was transferred to DMEM for cell culture. Subsequently, the cell-laden hydrogels were rinsed three times with phosphate buffered saline (PBS) and cultured in DMEM before being placed into the incubator. Additionally, cell proliferation on the surfaces of the PN and PN-GelMA hydrogel thin films postphotodegradation was examined. Cell proliferation was assessed at 0, 1, 3, and 7 days. C2C12-laden hydrogels were submerged in a 1:10 dilution of CCK-8 solution for 2 h within the incubator. The solution was then transferred to a 96-well plate, and absorbance at 450 nm was measured using a plate reader (SpectraMax M5, Molecular Devices, USA).

Live/Dead Staining and Fluorescence Tracking: Live and dead C2C12 cells were stained using the LIVE/DEAD Cell Vitality Kits (Invitrogen, USA). The cell-laden hydrogel was incubated for 1 h after fabrication. Following incubation, the hydrogel was washed with TBS and immersed in the calcein AM/ethidium homodimer-1 solution for ≈ 15 min. Subsequently, the samples were excited at 488 and 514 nm wavelengths and visualized using a fluorescence microscope (Leica DM IRB).

C2C12 cells were labeled with a green fluorescent cell tracker, PKH67 (Sigma-Aldrich, USA). Subsequently, the labeled C2C12 cells were cultured in PN-GelMA hydrogels for 0 h (after photocrosslinking) and 1 day (after swelling), and cell adhesion and proliferation were observed using a fluorescence microscope (Leica DM IRB). The green fluorescence emitted by the labeled cells was detected within the range of 610–750 nm.

Statistical Analysis: All experiments were performed three times independently. Data in this study were presented as mean \pm standard deviation. Statistical analysis was carried out using the Student's *t*-test, and statistical significance was determined for results with *p* values less than 0.05.

Supporting Information

Supporting Information is available from the Wiley Online Library or from the author.

Acknowledgements

This work was supported by the National Science and Technology Council, Taiwan, R.O.C. (NSTC 112-2221-E-002-056-MY3). The beginning study of this work was carried out with the support of Prof. Levkin's group at Karlsruhe Institute of Technology. P.A.L. thanks the Deutsche Forschungsgemeinschaft (DFG) for the financial support (Heisenbergprofessur project number 406232485, LE 2936/9-1). N.K.M. was funded by an internationalization Fellowship from the Carlsberg Foundation (CF21-0614). The authors thank Dr. Hsi-Ching Tseng at the NTU Instrumentation Center for the assistance in NMR experiments. We were obliged to the National Synchrotron Radiation Research Center (2023-1-137-2) and the TPS 25A beamline group for providing the resources and technical support.

Open Access funding enabled and organized by Projekt DEAL.

Conflict of Interest

The authors declare no conflict of interest.

Author Contributions

Qian-Pu Cheng: conceptualization (equal); formal analysis (lead); investigation (lead); methodology (equal); visualization (lead); writing—original draft (lead); writing—review & editing (equal). **Nikolaj K. Mandsberg:** funding acquisition (supporting); visualization (supporting); writing—review & editing (equal). **Pavel A. Levkin:** funding acquisition (supporting); methodology (equal); resources (equal); supervision (equal); writing—review & editing (equal). **Shan-hui Hsu:** conceptualization (equal); funding acquisition (lead); methodology (equal); resources (equal); supervision (equal); writing—review & editing (equal).

Data Availability Statement

The data that support the findings of this study are available in the supplementary material of this article.

Keywords

biocompatible actuators, photodegradations, photoresponsive hydrogels, programmable actuators, thermoresponsive hydrogels

Received: October 22, 2024

Revised: February 3, 2025

Published online:

- [1] I. Apsite, S. Salehi, L. Ionov, *Chem. Rev.* **2022**, *122*, 1349.
- [2] Q. Shi, H. Liu, D. Tang, Y. Li, X. Li, F. Xu, *NPG Asia Mater.* **2019**, *11*, 64.
- [3] M. C. Koetting, J. T. Peters, S. D. Steichen, N. A. Peppas, *Mater. Sci. Eng.: R Rep.* **2015**, *93*, 1.
- [4] X. Le, W. Lu, J. Zhang, T. Chen, *Adv. Sci.* **2019**, *6*, 1801584.
- [5] H. K. Yap, J. C. H. Goh, R. C. H. Yeow, in *6th European Conf. of the Int. Federation for Medical and Biological Engineering: MBEC 2014*, Springer, New York, NY **2015**, pp. 367–370.
- [6] Z. Zhang, Y. Wang, Q. Wang, L. Shang, *Small* **2022**, *18*, 2105116.
- [7] D. Qureshi, S. K. Nayak, S. Maji, A. Anis, D. Kim, K. Pal, *Eur. Polym. J.* **2019**, *120*, 109220.
- [8] N. El-Atab, R. B. Mishra, F. Al-Modaf, L. Joharji, A. A. Alsharif, H. Alamoudi, M. Diaz, N. Qaiser, M. M. Hussain, *Adv. Intell. Syst.* **2020**, *2*, 2000128.
- [9] P. Lavrador, M. R. Esteves, V. M. Gaspar, J. F. Mano, *Adv. Funct. Mater.* **2021**, *31*, 2005941.
- [10] G. Cirillo, T. Spataro, M. Curcio, U. G. Spizzirri, F. P. Nicoletta, N. Picci, F. Iemma, *Mater. Sci. Eng. C* **2015**, *48*, 499.
- [11] Y. Zhang, J. Yu, K. Ren, J. Zuo, J. Ding, X. Chen, *Biomacromolecules* **2019**, *20*, 1478.
- [12] E. Bellotti, A. L. Schilling, S. R. Little, P. Decuzzi, *J. Control. Release* **2021**, *329*, 16.
- [13] M. A. Haq, Y. Su, D. Wang, *Mater. Sci. Eng. C* **2017**, *70*, 842.
- [14] L. Li, J. M. Scheiger, P. A. Levkin, *Adv. Mater.* **2019**, *31*, 1807333.
- [15] D. Lu, M. Zhu, S. Wu, Q. Lian, W. Wang, D. Adlam, J. A. Hoyland, B. R. Saunders, *Adv. Funct. Mater.* **2020**, *30*, 1909359.
- [16] L. Dai, J. Lu, F. Kong, K. Liu, H. Wei, C. Si, *Adv. Compos. Hybrid Mater.* **2019**, *2*, 462.
- [17] J. R. Choi, K. W. Yong, J. Y. Choi, A. C. Cowie, *BioTechniques* **2019**, *66*, 40.
- [18] A. Rosenfeld, T. Göckler, M. Kuzina, M. Reischl, U. Schepers, P. A. Levkin, *Adv. Healthcare Mater.* **2021**, *10*, 2100632.
- [19] J. Shi, L. Yu, J. Ding, *Acta Biomater.* **2021**, *128*, 42.
- [20] H. Banerjee, M. Suhail, H. Ren, *Biomimetics* **2018**, *3*, 15.
- [21] Y. Zhang, Y. Huang, *Front. Chem.* **2021**, *8*, 615665.
- [22] F.-M. Cheng, H.-X. Chen, H.-D. Li, *J. Mater. Chem. B* **2021**, *9*, 1762.
- [23] X. Liu, J. Liu, S. Lin, X. Zhao, *Mater. Today* **2020**, *36*, 102.
- [24] K. Mendez, W. Whyte, B. R. Freedman, Y. Fan, C. E. Varela, M. Singh, J. C. Cintron-Cruz, S. E. Rothenbücher, J. Li, D. J. Mooney, *Adv. Mater.* **2023**, *2303301*.
- [25] M. Filippi, T. Buchner, O. Yasa, S. Weirich, R. K. Katzschmann, *Adv. Mater.* **2022**, *34*, 2108427.
- [26] J. M. Scheiger, S. Li, M. Brehm, A. Bartschat, P. Theato, P. A. Levkin, *Adv. Funct. Mater.* **2021**, *31*, 2105681.
- [27] Y.-C. Huang, Q.-P. Cheng, U.-S. Jeng, S.-H. Hsu, *ACS Appl. Mater. Interfaces* **2023**, *15*, 5798.
- [28] J. M. Scheiger, P. A. Levkin, *Adv. Funct. Mater.* **2020**, *30*, 1909800.
- [29] D. Lu, M. Zhu, W. Wang, S. Wu, B. R. Saunders, D. J. Adlam, J. A. Hoyland, C. Hofzumahaus, S. Schneider, K. Landfester, *Soft Matter* **2019**, *15*, 527.
- [30] G. A. El-Hiti, D. S. Ahmed, E. Yousif, O. S. Al-Khazrajy, M. Abdallah, S. A. Alanazi, *Polymers* **2021**, *14*, 20.
- [31] J. Li, Q. Ma, Y. Xu, M. Yang, Q. Wu, F. Wang, P. Sun, *ACS Appl. Mater. Interfaces* **2020**, *12*, 55290.

- [32] W. Liu, L. Geng, J. Wu, A. Huang, X. Peng, *Compos. Sci. Technol.* **2022**, 225, 109494.
- [33] X.-X. Le, Y.-C. Zhang, W. Lu, L. Wang, J. Zheng, I. Ali, J.-W. Zhang, Y.-J. Huang, M. J. Serpe, X.-T. Yang, X.-D. Fan, T. Chen, *Macromol. Rapid Commun.* **2018**, 39, 1800019.
- [34] K. Cho, D. Kang, H. Lee, W.-G. Koh, *Chem. Eng. J.* **2022**, 427, 130879.
- [35] D. Jiao, Q. L. Zhu, C. Y. Li, Q. Zheng, Z. L. Wu, *Acc. Chem. Res.* **2022**, 55, 1533.
- [36] Y. Dong, J. Wang, X. Guo, S. Yang, M. O. Ozen, P. Chen, X. Liu, W. Du, F. Xiao, U. Demirci, *Nat. Commun.* **2019**, 10, 4087.
- [37] Z. Jiang, S. M. Seraji, X. Tan, X. Zhang, T. Dinh, M. Mollazade, A. E. Rowan, A. K. Whittaker, P. Song, H. Wang, *Chem. Mater.* **2021**, 33, 7818.
- [38] a) N. Shi, Y. Li, L. Chang, G. Zhao, G. Jin, Y. Lyu, G. M. Genin, Y. Ma, F. Xu, *Small Methods* **2021**, 5, 2100276. b) J. Wang, A. Khodabukus, L. Rao, K. Vandusen, N. Abutaleb, N. Bursac, *Biomaterials* **2019**, 221, 119416.
- [39] J. Wang, A. Khodabukus, L. Rao, K. Vandusen, N. Abutaleb, N. Bursac, *Biomaterials* **2019**, 221, 119416.
- [40] O. R. Tonti, H. Larson, S. N. Lipp, C. M. Luetkemeyer, M. Makam, D. Vargas, S. M. Wilcox, S. Calve, *Acta Biomater.* **2021**, 132, 83.
- [41] M. Nan, K. Guo, T. Jia, G. Wang, S. Liu, *ACS Appl. Mater. Interfaces* **2024**, 16, 9224.
- [42] M. Chen, Y. Cui, Y. Wang, C. Chang, *Chem. Eng. J.* **2023**, 453, 139893.
- [43] L. Zhang, H. Yan, J. Zhou, Z. Zhao, J. Huang, L. Chen, Y. Ru, M. Liu, *Adv. Mater.* **2023**, 35, 2202193.
- [44] D. Lu, Q. Lian, M. Zhu, *Adv. Sci.* **2024**, 11, 2304776.
- [45] N. Park, J. Kim, *Adv. Intell. Syst.* **2020**, 2, 1900135.
- [46] J. Z. Hilt, *J. Polym. Sci. Part A: Polym. Chem.* **2010**, 48, 3229.
- [47] H. Shirahama, B. H. Lee, L. P. Tan, N.-J. Cho, *Sci. Rep.* **2016**, 6, 31036.